

Article

High Catalytic Efficiency of Nanostructured β -CoMoO₄ in the Reduction of the *Ortho*-, *Meta*- and *Para*-Nitrophenol Isomers

Fahd Al-Wadaani¹, Ahmed Omer¹, Mostafa Abboudi¹, Hicham Oudghiri Hassani^{1,2,*}, Souad Rakass¹, Mouslim Messali¹ and Mohammed Benaissa³

¹ Chemistry Department, College of Science, Taibah University, Almadinah 30002, Saudi Arabia; fwadaani@taibahu.edu.sa (F.A.-W.); ahmed.hussein.omer@gmail.com (A.O.); abboudi14@hotmail.com (M.A.); rakass_souad@yahoo.fr (S.R.); aboutasnim@yahoo.fr (M.M.)

² Département Sciences de la Nature, Cégep de Drummondville, 960 Rue Saint-Georges, Drummondville, QC J2C 6A2, Canada

³ LMPHE, Département de Physique, Faculté des Sciences, Université Mohammed V, B.P. 1014 RP, Rabat 10000, Morocco; benaissa.um5@gmail.com

* Correspondence: Oudghiri_hassani_hicham@yahoo.com; Tel.: +966-543-549-454

Received: 8 January 2018; Accepted: 7 February 2018; Published: 9 February 2018

Abstract: Nanostructured β -CoMoO₄ catalysts have been prepared via the thermal decomposition of an oxalate precursor. The catalyst was characterized by infrared spectroscopy (FTIR), X-ray diffraction (XRD), Brunauer-Emmett-Teller method (BET), energy dispersive X-ray spectroscopy (EDX), and transmission electron microscopy (TEM). The efficiency of these nanoparticles in the reduction of *ortho*- and *meta*-nitrophenol isomers (2-NP, 3-NP, and 4-NP) to their corresponding aminophenols was tested using UV-visible spectroscopy measurements. It was found that, with a β -CoMoO₄ catalyst, NaBH₄ reduces 3-NP instantaneously, whilst the reduction of 2-NP and 4-NP is slower at 8 min. This difference is thought to arise from the lower acidity of 3-NP, where the negative charge of the phenolate could not be delocalized onto the oxygen atoms of the meta-nitro group.

Keywords: nanostructures; β -CoMoO₄; nitrophenol reduction; nanoparticles

1. Introduction

Aminophenols are implicated in the synthesis of pharmaceutically active compounds [1]. For instance, *p*-aminophenol is an important intermediate in the preparation of several analgesic and antipyretic drugs, such as paracetamol, acetanilide, and phenacetin [2]. In addition, aminophenols are key ingredients in the production of metal-complex dyes and are used in corrosion inhibition, hair-dyeing agents, and polymer production [1,2]. Due to their diverse applications, the development of efficient processes for the synthesis of aminophenols has gained increasing attention.

One method of synthesizing aminophenols is via the reduction of nitrophenols. Nanostructured transition metal molybdate materials have shown promise as catalysts for this process [3,4]. In particular, nanostructured CoMoO₄ provides a non-toxic and inexpensive candidate for this process [5]. CoMoO₄, which may exist in several phases including a low temperature α -phase and a high temperature β -phase, [3,5–7] is used as a catalyst in many chemical [8] and petrochemical processes such as cracking, hydrogenation, dehydrogenation, and hydrodesulfurization (HDS) [6,9]. The catalytic properties of CoMoO₄ depend on the structure of the material, which in turn depends on the method of preparation [10]. Various methods have been developed for the synthesis of CoMoO₄ including precipitation, sol-gel, solid state reaction, hydrothermal, complete evaporation of a polymer-based metal-complex precursor solution, microemulsion and sonochemical [11–16].

Several materials were tested in the reduction reaction of the nitrophenol isomers. The ferrites materials CuFe_2O_4 and NiFe_2O_4 were studied by Goyal et al. and found that the copper containing ferrite was a better catalyst for these reactions [17]. Moreover, Nandanwar et al. investigated the efficiency of $\text{CuO}/\gamma\text{Al}_2\text{O}_3$, which showed good catalytic activity [18]. Ni/C black composite material was also tested as a catalyst for this reaction by Xia et al., and low efficiency was observed [19]. Better results were found in a study conducted by Oudghiri on the iron molybdate $\text{Fe}_2(\text{MoO}_4)_3$ [20]. Ghorai et al. worked with a mixed molybdate phosphate of cobalt, copper, and chromium that was were found to efficiently reduce 4-NP [21]. In recent years, the application of CoMoO_4 to the catalytic degradation of organic dyes has started to receive increasing attention. For instance, CoMoO_4 nanoparticles prepared via the microemulsion method have been shown to be quite effective at eliminating reactive black (RB) 8 dye from aqueous solution, with a decolorization efficiency of 91.47% [12].

In this study, nanostructured $\beta\text{-CoMoO}_4$ catalysts were prepared via the thermal decomposition of an oxalate precursor prepared in the solid state using a new method. The obtained powder was found to be formed of nanoparticles. The freshly synthesized $\beta\text{-CoMoO}_4$ nanoparticles were tested as catalysts in the reduction of three aminophenol isomers (2-NP, 3-NP, and 4-NP) to their corresponding aminophenol isomers.

2. Material and Methods

2.1. Materials

Cobalt nitrate ($\text{Co}(\text{NO}_3)_2 \cdot 6\text{H}_2\text{O}$), ammonium molybdate ($(\text{NH}_4)_6\text{Mo}_7\text{O}_{24} \cdot 4\text{H}_2\text{O}$), and oxalic acid ($\text{H}_2\text{C}_2\text{O}_4 \cdot 2\text{H}_2\text{O}$) were obtained from Aldrich (St. Louis, MO, USA). All the chemicals were of analytical grade and used without further purification.

2.2. Catalyst Preparation

The cobalt molybdate catalyst (CoMoO_4) was prepared by thermal decomposition of an oxalate precursor in a tubular furnace (open on both sides) at $550\text{ }^\circ\text{C}$ for 2 h. The oxalate precursor was obtained by the solid state reaction of a well-ground mixture of cobalt nitrate ($\text{Co}(\text{NO}_3)_2 \cdot 6\text{H}_2\text{O}$), ammonium molybdate ($(\text{NH}_4)_6\text{Mo}_7\text{O}_{24} \cdot 4\text{H}_2\text{O}$), and oxalic acid ($\text{H}_2\text{C}_2\text{O}_4 \cdot 2\text{H}_2\text{O}$) in the molar ratio 1:1/7:5, respectively, on a hotplate at $160\text{ }^\circ\text{C}$ for 1 h [22]. During heating, an orange/brownish gas is evolved, indicating the formation of NO_2 gas due to the reduction of the nitrate anions. In the meantime, the mixture takes a dark blue coloration confirming the reduction of the molybdenum (+VI) to lower oxidation states (+V or +IV). The oxalic acid acted not only as a reducing agent but also as a complexing agent leading to the formation of the oxalate complexes of the existing metals [23,24]. The advantage of this preparation method is that it occurs in the solid state without adding any solvent. There is no factor to control other than the temperature of the precursor formation at $160\text{ }^\circ\text{C}$ and the heating temperature at $550\text{ }^\circ\text{C}$. No strict conditions such as higher temperatures or pressures are needed. Moreover, the time of the preparation of the nanoparticles is limited to a few hours with a yield of almost 100%. All synthesis methods encountered in the literature require the use of solvents for the filtration and drying stages. In the solid-state reaction between MoO_3 and Co_3O_4 , higher temperatures as well as regrinding mixture and annealing stages are needed to obtain improved homogeneity.

2.3. Characterization

In order to study the decomposition with temperature of the prepared oxalate precursor, thermal analyses were conducted on an SDT Q600 instrument (Ta Instruments, Hayesville, NC, USA). Infrared spectroscopy studies were conducted on a Shimadzu 8400S (Shimadzu, Tokyo, Japan), to confirm the oxalate complex formation. To verify the crystallinity and the purity of the prepared cobalt molybdate, the X-ray diffraction patterns were recorded on a Shimadzu X-ray diffractometer 6000 (Shimadzu, Tokyo, Japan), using $\text{Cu K}\alpha$ radiation (1.5406 \AA equipped with a Ni filter). The patterns

were recorded in the range of 10–80° in 2 θ . Crystallites size was calculated using the Scherer formula $D_{\text{XRD}} = 0.9 \lambda / (B \cos\theta)$, where λ is the Cu K α wavelength, B is the full width at half maximum (FWHM) expressed in radians, and θ is the Bragg angle. Particle sizes could also be estimated using the equation $D_{\text{BET}} = 6000/d.S$, where d is the density and S is the specific surface area calculated from the adsorption/desorption isotherms that were obtained from a Micromeritics ASAP 2020 (Micromeritics, Norcross, GA, USA), surface area and porosity analyzer. The variation of the nitrophenol isomer (2-NP, 3-NP and 4-NP) concentrations during the catalytic transformation to their corresponding aminophenol isomers was measured using a Varian Cary 100 UV-visible spectrophotometer (Varian Inc., Palo Alto, CA, USA). Transmission electron microscopy (TEM) was performed using a Tecnai-12 electron microscope (FEI, Hillsboro, OR, USA), operated at 120 kV to investigate the shape and size of the particles. For the TEM measurement, the sample was prepared by simply grinding the powder between two glass plates and bringing the fine powder into contact with a carbon-coated copper TEM grid. Energy dispersive X-ray (EDX) microanalyses were obtained using an EDAX detector coupled to a TEM instrument.

2.4. General Procedure for the Reduction of Nitrophenol Isomers

The prepared cobalt molybdate powder was tested as a catalyst in the reduction of three nitrophenol isomers (2-NP, 3-NP, and 4-NP) to their corresponding aminophenol isomers. In a typical test, 40 mL of an 8×10^{-4} M aqueous solution of sodium tetrahydroborate (NaBH₄) were added to 40 mL of a 4×10^{-4} M aqueous solution of the nitrophenol isomer under continuous stirring at ambient temperature. The solution color immediately became dark yellow, with an absorption located at 415, 393, and 401 nm for the *ortho*-isomer (2-NP), the *meta*-isomer (3-NP), and the *para*-isomer (4-NP), respectively, due to the resonance stabilization of the formed nitrophenolate anions. One hundred milligrams of the cobalt molybdate catalyst was then added to the mixture under continuous stirring. The reaction was monitored via UV visible spectroscopy measurements. Absorbance intensity decreases as nitrophenolate anion concentration decreases, thus allowing us to use this relationship as a measure of the efficiency of the catalyst in this reduction reaction.

3. Results and Discussion

3.1. Complex Precursor Characterizations

As the first step, the product of the solid state reaction between the mixture of Co(NO₃)₂·6H₂O and the ammonium molybdate ((NH₄)₆Mo₇O₂₄·4H₂O) with the oxalic acid was studied by infrared spectroscopy. The FTIR spectrum of the resulting complex is shown in Figure 1. The spectrum is similar to previous studies for oxalate complexes [25–28]. The bands at 920 and 963 cm⁻¹ are assigned to the Mo=O stretching, the 1360 and 1317 cm⁻¹ region can be assigned to $\nu(\text{C-O})$ and $\delta(\text{OCO})$, and the 1402 cm⁻¹ band to the C-O stretching [28]. The spectrum also reveals the presence of a large band in the range of 1800–1550 cm⁻¹. The deconvolution of this band shows bands at 1731 and 1675 cm⁻¹, which can be assigned to the C=O vibration of the oxalate group [27,28] and a band at 1635 cm⁻¹ corresponding to $\delta(\text{H}_2\text{O})$ [26]. At high frequency, the spectrum reveals a broad intense band in the 2850–3750 cm⁻¹ range. The deconvolution of this broad band reveals bands at 3385 cm⁻¹, which can be attributed to the OH bridging group between two metal ions [29], and at 3170 cm⁻¹, which can be attributed to the stretching vibration of NH₄⁺ ion [29,30]. Furthermore, a band at 1240 cm⁻¹ can be attributed to $\delta(\text{NH}_4^+)$ and confirm therefore the presence of the NH₄⁺ group in the precursor [30]. These results permit the conclusion that an oxalate complex, containing oxo molybdenum units, hydroxyl (-OH), water, and NH₄⁺ ion, was formed. The results from the thermal analysis (TGA and DTA) studies are presented in Figure 2. The TG curve is divided in four parts with a total weight loss of 44.1% between room temperature and 380 °C. The first weight loss of 4.4% can be attributed to the crystallization water. Moreover, the second and third weight losses located between 170 and 300 °C can be attributed to the decomposition of the complex. Finally, a last

small loss of 2.1% is observed between 300 and 375 °C. A similar loss in the same range was obtained in a previous study of bismuth oxalate complex containing an OH group and can be attributed to this OH group [31,32]. By compiling the results obtained by FTIR, TGA, and the possible oxidation degree of cobalt and molybdenum, a formula of the oxalate complex can be suggested as $(\text{NH}_4)\text{CoMoO}(\text{C}_2\text{O}_4)_2(\text{OH})\cdot\text{H}_2\text{O}$. The total weight loss observed is 44.1% in comparison with the theoretical value of 45.3% for the suggested formula. This complex was subsequently thermally decomposed in air at a chosen temperature of 550 °C to obtain the resulting oxide phase.

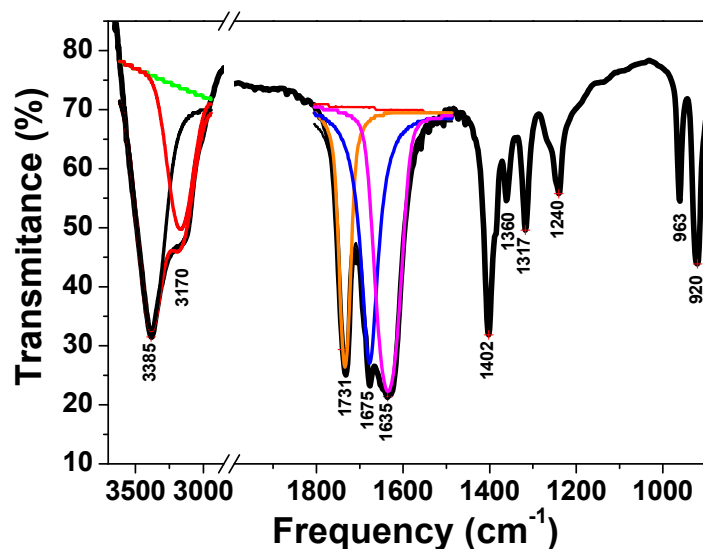


Figure 1. FTIR spectrum of the as-prepared oxalate precursor.

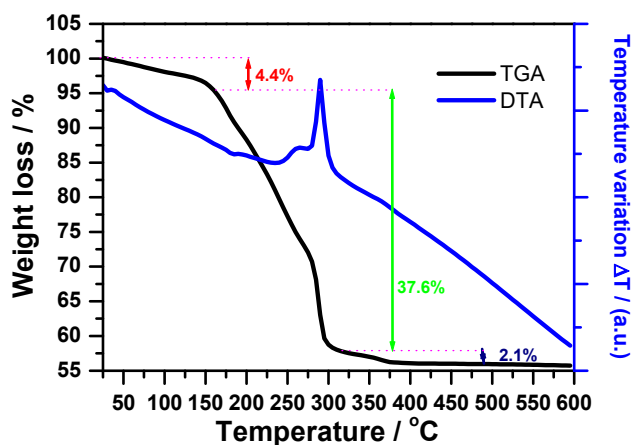


Figure 2. TGA and DTA thermograms recorded under air.

3.2. Cobalt Molybdate Characterization

3.2.1. X-ray Diffraction

The X-ray diffraction pattern of the powder prepared via this new and original method is given in Figure 3. A pure phase CoMoO_4 was obtained. All the observed peaks could be indexed in accordance with the J.C.P.D.S. file # 21-0868. The CoMoO_4 crystallizes in the monoclinic cell in the space group C2/m with the parameters: $a = 10.21$, $b = 9.268$, $c = 7.022$, and $\beta = 106.9^\circ$. The crystallites size was calculated using the Debye–Scherer equation, assuming that the crystallites have a spherical shape. A separate diffraction peak (021) was considered for this calculation ($2\theta = 23.22^\circ$). The crystallites size was found to be 17.6 nm.

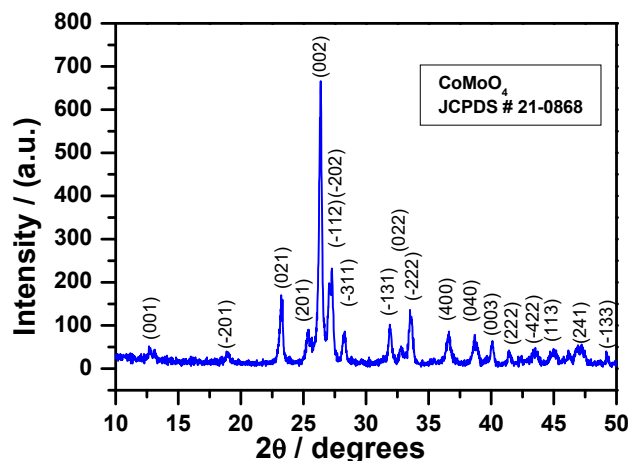


Figure 3. XRD pattern of the β -CoMoO₄ nanoparticle powder obtained after calcination of the oxalate precursor at 550 °C.

3.2.2. Specific Surface Area Measurement

The synthesized cobalt molybdate (CoMoO₄) has a BET surface of 28.35 m²/g, which corresponds to a particle size of 46.3 nm calculated using the equation $D_{\text{BET}} = 6000/d \cdot S$, where d is the density and S is the specific surface area. It is a higher value than that calculated from the XRD pattern. On the other hand, as depicted in Figure 4, the adsorption/desorption isotherms are type IV exhibited by mesoporous solids and exhibit the characteristic H1 hysteresis loop (IUPAC classification), which is consistent with mesoporous or nanoporous materials [33,34]. The pores are cylindrical or slit shaped. The pore size was found to be of 18.8 nm, and the total pore volume found to be 0.1336 cm³/g using the BJH (Barrett-Joyner-Halenda) method.

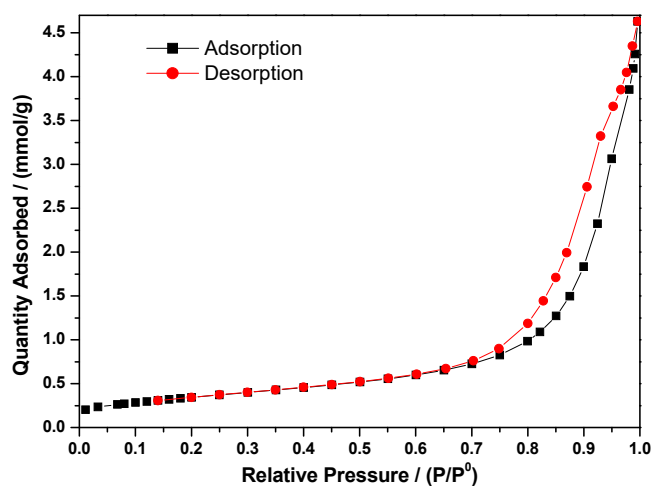


Figure 4. Adsorption and desorption curves obtained from the BET measurements of the β -CoMoO₄ nanoparticles.

3.2.3. Transmission Electron Microscopy

Micrographs of the β -CoMoO₄ nanoparticles were taken at low magnification showing agglomerated nanoparticles (Figure 5a). The agglomerates are about one micron in size. At higher magnification, the particle size found is in the range between 20 and 40 nm (Figure 5b,c). This value is lower than obtained from BET study (46.3 nm). This result can be explained by the fact that in BET, agglomerated particles offer less surface for the adsorption-desorption phenomena, so the

calculated particle size is higher. The calculated particle size using the Scherer formula from XRD study (17.6 nm) was found lower than those found in either BET or TEM observation. This is because what was calculated was the crystallite size, which was smaller than the particle size.

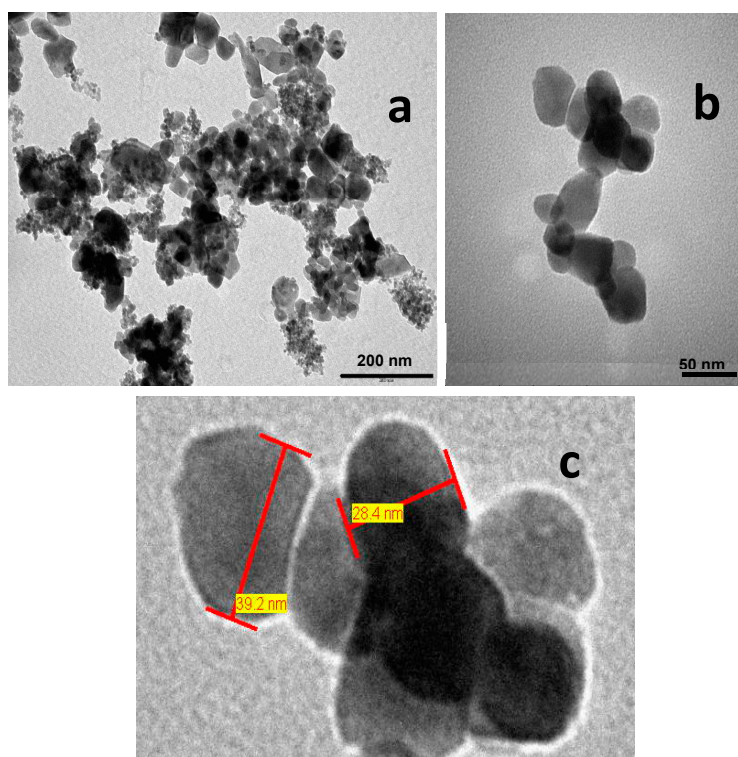


Figure 5. The TEM micrographs of the as-prepared β -CoMoO₄ powder (a) at low magnification ($\times 100,000$), scale bar 200 nm; and (b) at high magnification ($\times 500,000$), scale bar 50 nm; (c) Measured particle size at high magnification.

In order to confirm the atomic composition and proportion in the β -CoMoO₄ nanoparticles, a study with EDX spectroscopy was performed. Figure 6 shows the results. The abundance of oxygen, cobalt, and molybdenum were found to be of 67.71%, 15.47%, and 16.82% compared to the theoretical values 66.67, 16.67, and 16.67 respectively.

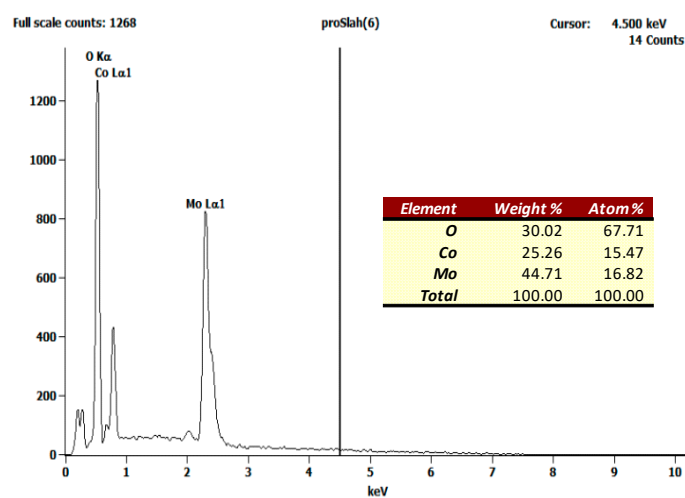


Figure 6. EDX spectrum of the as synthesized β -CoMoO₄ and its atomic abundance.

3.3. Reduction of Nitrophenol Isomers

The results of the catalytic reduction study are shown in Figure 7. As is clear, the efficiency of the β -CoMoO₄ catalyst is remarkable. An instantaneous reduction happened in the case of 3-NP (Figure 7a). In contrast, the reduction reaction was slower in the case of 2-NP and 4-NP (8 min). This difference in efficiency is probably due to a higher basic character of 3-NP, where the mesomeric conjugation is more important.

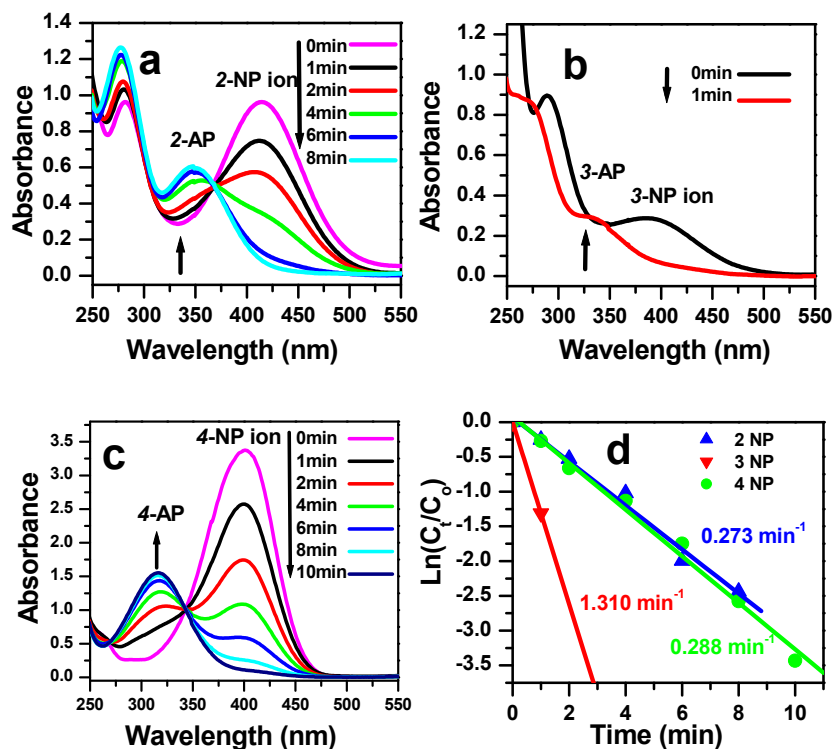


Figure 7. Successive UV-vis spectra of the reduction of (a) 2-nitrophenol solution (4×10^{-4} M); (b) 3-nitrophenol solution (4×10^{-4} M); (c) 4-nitrophenol solution (4×10^{-4} M) in the presence of 8×10^{-4} M NaBH₄ using β -CoMoO₄ nanocatalyst (0.1 g); (d) Plot of $\ln(C/C_0)$ against reaction time for the nitrophenol isomers in the presence of β -CoMoO₄ and determination of the reduction reaction rate constant k_{app} .

An experiment was conducted to study the influence of the NaBH₄ concentration on the rate constant of the reduction reaction. Different concentrations were taken for NaBH₄ maintaining the same conditions as described in the protocol. When the concentration was increased to NaBH₄/NP ratios of 50:1, 25:1, 12.5:1, and 5:1, the catalyst was decomposed by the hydride. However, when a 2:1 ratio was used, the catalyst did not react with NaBH₄. These were the optimal conditions for this reaction.

On the other hand, the catalyst recycling was studied for 3-NP, where a faster reduction time was observed. After the reduction test, the solution was filtered and the powder recuperated. After thorough washing with water, the powder was left to dry at 80 °C overnight and used in the next recycling test, conserving the same experimental conditions operated in the first reduction test. The recycling was repeated four times, and the results are represented in Figure 8. The reduction time of 1 min did not change in any the recycling tests, showing the good stability of the β -CoMoO₄ nanocatalyst in this type of reduction reaction.

It is important to compare the relative reaction kinetics of the 2-NP, 3-NP, and 4-NP reduction for the catalysts synthesized in this work and those reported in the literature for other catalysts. The results are summarized in Table 1.

Importantly, this is the first time that such a high catalytic efficiency has been observed for a low-cost nanocatalyst and highly concentrated solutions of nitrophenol isomers. The observed rate constant for the simultaneous reduction of the 3-NP isomer for the β -CoMoO₄ catalyst is relatively high and is of 1.310 min⁻¹. However, definite conclusions cannot be reached from these comparisons due to the differences in the experimental conditions, such as the NaBH₄/NP/catalyst equivalent ratio and the temperature or the reactants concentration. On the other hand, the reaction time is also a good criterion of efficiency and in our case the reaction is instantaneous. Goyal et al. have reported a similar efficiency [17] but for a lower concentration of the nitrophenol. One important point is that the reduction of the 3-NP isomer is faster than the reduction of the 2-NP isomer by approximately one order of magnitude (8/1) and the reverse situation is observed in the work of Goyal et al. This suggests that the reduction reaction mechanism is different for the β -CoMoO₄ and CuFe₂O₄ catalysts.

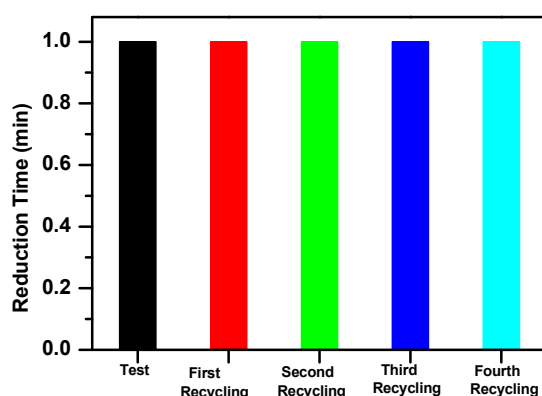


Figure 8. Recycled catalyst against reduction time in the reduction of 3-NP with NaBH₄ catalyzed with β -CoMoO₄ nanoparticles.

Table 1. Pseudo-first order rate constants for the reduction of 2-NP, 3-NP, and 4-NP by CoMoO₄ with other nanocatalysts reported in the literature.

Catalyst	Type	Concentration of NP (mol/L)	Reaction Time (min)	Rate Constant (min ⁻¹)	References
CoMoO ₄	Nanoparticles	2×10^{-4}	8	0.273 for 2-NP	This work
			1	1.310 for 3-NP	
			8	0.288 for 4-NP	
CuFe ₂ O ₄	Nanoparticles	3.6×10^{-5}	3	3.676 for 2-NP	[17]
			1.5	0.983 for 3-NP	
			3	0.846 for 4-NP	
NiFe ₂ O ₄	Nanoparticles	3.6×10^{-5}	20	0.327 for 2-NP	[17]
			12	0.062 for 3-NP	
			16	0.118 for 4-NP	
CuO/ γ -Al ₂ O ₃	Nanocomposites	2.9×10^{-5}	15	— for 2-NP	[18]
			20	— for 3-NP	
			12	0.174 for 4-NP	
Ni/C black	Nanocomposites	5.0×10^{-4}	15	0.594 for 2-NP	[19]
			15	0.594 for 3-NP	
			15	0.5970 for 4-NP	
Fe ₂ (MoO ₄) ₃	Nanoparticles	2×10^{-4}	12	0.160 for 2-NP	[20]
			4	0.427 for 3-NP	
			9	0.323 for 4-NP	

4. Conclusions

β -CoMoO₄ nanostructures with a high catalytic efficiency in the reduction of *ortho*-, *meta*-, and *para*-nitrophenol isomers to their corresponding aminophenols have been successfully prepared

via the thermal decomposition of an oxalate precursor. The reduction was instantaneous in the case of 3-NP but quite a bit slower in the cases of 2-NP and 4-NP (8 min). This difference in efficiency is probably due to the higher basicity of 3-NP. A recycling test on the reduction of 3-NP showed the stability of the nanocatalyst and its high efficiency even after four cycles.

Acknowledgments: This work was supported financially by the Research Deanship of Taibah University under Grant No. 435/6426).

Author Contributions: M.A. and H.O.H. conceived and designed the experiments; all the authors performed the experiments and analyzed the data; M.A., H.O.H. and A.O. wrote the paper.

Conflicts of Interest: The authors declare no conflict of interest.

References

1. Yang, P.; Xua, A.; Xiab, J.; Hea, J.; Xinga, H.; Zhanga, X.; Weia, S.; Wang, N. Facile synthesis of highly catalytic activity Ni-Co-Pd-P composite for reduction of the *p*-Nitrophenol. *Appl. Catal. A-Gen.* **2014**, *470*, 89–96. [[CrossRef](#)]
2. Laksmia, B.; Shivanandaa, K.N.; Mahendraa, K.N.; Gowdab, N.M.; Jagadeesha, R.V. An efficient platinum-catalyzed oxidation process and mechanism for the facile conversion of benzoxazoles to aminophenols. *Chem. Eng. J.* **2010**, *163*, 403–412. [[CrossRef](#)]
3. Rico, J.L.; Avalos-Borja, M.; Barrera, A.; Hargreaves, J.S.J. Template-free synthesis of CoMoO₄ rods and their characterization. *Mater. Res. Bull.* **2013**, *48*, 4614–4617. [[CrossRef](#)]
4. Rosić, M.; Zarubica, A.; Šaponjić, A.; Babić, B.; Zagorac, J.; Jordanov, D.; Matović, B. Structural and photocatalytic examination of CoMoO₄ nanopowders synthesized by GNP method. *Mater. Res. Bull.* **2018**, *98*, 111–120. [[CrossRef](#)]
5. Shaoqing, Y.; Jun, H.; Jianlong, W. Radiation-induced catalytic degradation of *p*-nitrophenol (PNP) in the presence of TiO₂ nanoparticles. *Radiat. Phys. Chem.* **2010**, *79*, 1039–1046. [[CrossRef](#)]
6. Rodriguez, J.A.; Hanson, J.C.; Chaturvedi, S.; Brito, J.L. Characterization of oxide catalysts using time-resolved XRD and XANES: Properties of pure and sulfided CoMoO₄ and NiMoO₄. *Stud. Surf. Sci. Catal.* **2000**, *130*, 2795–2800.
7. Zagorac, D.; Schon, J.C.; Rosic, M.; Zagorac, J.; Jordanov, D.; Lukovic, J.; Matovic, B. Theoretical and Experimental Study of Structural Phases in CoMoO₄. *Cryst. Res. Technol.* **2017**, *52*, 1700069. [[CrossRef](#)]
8. Unnarkat, A.P.; Sridhar, T.; Mahajani, S.M.; Suresh, A.K. Study of Cobalt Molybdenum Oxide Supported on Mesoporous Silica for Liquid Phase Cyclohexane Oxidation. *Catal. Today* **2017**, in press. [[CrossRef](#)]
9. Sen, A.; Pramanik, P. Low-temperature synthesis of nano-sized metal molybdate powders. *Mater. Lett.* **2001**, *10*, 287–294. [[CrossRef](#)]
10. Brito, J.L.; Barbosa, A.L. Effect of Phase Composition of the Oxidic Precursor on the HDS Activity of the Sulfided Molybdates of Fe(II), Co(II), and Ni(II). *J. Catal.* **1997**, *171*, 467–475. [[CrossRef](#)]
11. Veerasubramani, G.K.; Krishnamoorthy, K.; Radhakrishnan, S.; Kim, N.; Kim, S.J. Synthesis, characterization, and electrochemical properties of CoMoO₄ nanostructures. *Int. J. Hydrog. Energy* **2014**, *39*, 5186–5193. [[CrossRef](#)]
12. Edrissi, M.; Samadaniyan-Isfahani, S.; Soleymani, M. Preparation of cobalt molybdate nanoparticles; Taguchi optimization and photocatalytic oxidation of Reactive Black 8 dye. *Powder Technol.* **2013**, *249*, 378–385. [[CrossRef](#)]
13. Fan, Y.; Ma, W.; He, J.; Du, Y. CoMoO₄ as a novel heterogeneous catalyst of peroxymonosulfate activation for the degradation of organic dyes. *RSC Adv.* **2017**, *7*, 36193–36200. [[CrossRef](#)]
14. Koo Kim, J.; Hwa Kim, J.; Chan Kang, Y. Electrochemical Properties of Multicomponent Oxide and Selenide Microspheres Containing Co and Mo Components with Several Tens of Vacant Nanorooms Synthesized by Spray Pyrolysis. *Chem. Eng. J.* **2018**, *333*, 665–677. [[CrossRef](#)]
15. Zhao, J.; Ren, X.; Ma, H.; Sun, X.; Zhang, Y.; Yan, T.; Wei, Q.; Wu, D. Synthesis of Self-supported Amorphous CoMoO₄ Nanowire Array for Highly Efficient Hydrogen Evolution Reaction. *Sustain. Chem. Eng.* **2017**, *5*, 10093–10098. [[CrossRef](#)]
16. Dam, D.T.; Huang, T.; Lee, J.M. Ultra-small and low crystalline CoMoO₄ nanorods for electrochemical capacitors. *Sustain. Energy Fuels* **2017**, *1*, 324–335. [[CrossRef](#)]

17. Goyal, A.; Bansal, S.; Singhal, S. Facile reduction of nitrophenols: Comparative catalytic efficiency of MFe_2O_4 ($M = Ni, Cu, Zn$) nano ferrites. *Int. J. Hydrogen Energy* **2014**, *39*, 4895–4908. [CrossRef]
18. Nandanwar, S.U.; Chakraborty, M. Synthesis of Colloidal $CuO/\gamma-Al_2O_3$ by Microemulsion and Its Catalytic Reduction of Aromatic Nitro Compounds. *Chin. J. Catal.* **2012**, *33*, 1532–1541. [CrossRef]
19. Xia, J.; He, G.; Zhang, L.; Sun, X.; Wang, X. Hydrogenation of nitrophenols catalyzed by carbon black-supported nickel nanoparticles under mild conditions. *Appl. Catal. B-Environ.* **2016**, *180*, 408–415. [CrossRef]
20. Oudghiri-Hassani, H. Synthesis, characterization and catalytic performance of iron molybdate $Fe_2(MoO_4)_3$ nanoparticles. *Catal. Commun.* **2015**, *60*, 19–22. [CrossRef]
21. Ghorai, T.K.; Dhak, D.; Azizan, A.; Pramanik, P. Investigation of phase formation temperature of nano-sized solid solution of copper/cobalt molybdate and chromium-phosphate ($M^1_xCr_{1-x}Mo_xP_{1-x}O_4$) [$M^1 = Co, Cu$]. *Mater. Sci. Eng. B* **2005**, *121*, 216–223. [CrossRef]
22. Kadiri, N.; Ben Ali, A.; Abboudi, M.; Moran, E. A new synthesis method to produce oxalate complexes: Cases of copper and lanthanum oxalates. *Phys. Chem. News* **2008**, *44*, 11–14.
23. Abboudi, M.; Messali, M.; Kadiri, N.; Ben Ali, A.; Moran, E. Synthesis of CuO, La_2O_3 , and La_2CuO_4 by the Thermal-Decomposition of Oxalates Precursors Using a New Method. *Synth. React. Inorg. Met.-Org. Nano* **2011**, *41*, 683–688. [CrossRef]
24. Messali, M.; Al Wadaani, F.; Oudghiri-Hassani, H.; Rakass, S.; Al Amri, S.; Benaissa, M.; Abboudi, M. Preparation, characterization and photocatalytic activity of hexagonal ZnO nanoparticles. *Mater. Lett.* **2014**, *128*, 187–190. [CrossRef]
25. Gabal, M.A.; El-Bellihi, A.A.; El-Bahnasawy, H.H. Effect of calcination temperature on $Co(II)$ oxalate dehydrate-iron(II) oxalate dihydrate mixture: DTA–TG, XRD, Mössbauer, FT-IR and SEM studies (Part II). *Mater. Chem. Phys.* **2003**, *81*, 84–92. [CrossRef]
26. Angermann, A.; Topfer, J. Synthesis of nanocrystalline $Mn-Zn$ ferrite powders through thermolysis of mixed oxalates. *Ceram. Int.* **2011**, *37*, 995–1002. [CrossRef]
27. Ouyang, J.M.; Deng, S.P.; Zhou, N.; Tieke, B. Effect of tartrates with various counterions on the precipitation of calcium oxalate in vesicle solutions. *Colloids Surf. A* **2005**, *256*, 21–27. [CrossRef]
28. Ng, K.Y.S.; Zhou, X.; Gulari, E. Spectroscopic characterization of molybdenum oxalate in solution and on alumina. *J. Phys. Chem.* **1985**, *89*, 2477–2481. [CrossRef]
29. Mindru, I.; Gingasu, D.; Marinescu, G.; Patron, L.; Calderon-Moreno, J.M.; Bartha, C.; Andronescu, C.; Crisan, A. Cobalt chromite obtained by thermal decomposition of oxalate coordination compounds. *Ceram. Int.* **2014**, *40*, 15249–15258. [CrossRef]
30. Ramis, G.; Yi, L.; Busca, G. Ammonia activation over catalysts for the selective catalytic reduction of NO_x and the selective catalytic oxidation of NH_3 . An FT-IR study. *Catal. Today* **1996**, *28*, 373–380. [CrossRef]
31. Oudghiri-Hassani, H.; Rakass, S.; Al Wadaani, F.; Al Ghamdi, K.; Omer, A.; Messali, M.; Abboudi, M. Synthesis, characterization and photocatalytic activity of $\alpha-Bi_2O_3$ nanoparticles. *J. Taibah Univ. Sci.* **2015**, *9*, 508–512. [CrossRef]
32. Rivenet, M.; Roussel, P.; Abraham, F. One-dimensional inorganic arrangement in the bismuth oxalate hydroxide $Bi(C_2O_4)OH$. *J. Solid State Chem.* **2008**, *181*, 2586–2590. [CrossRef]
33. Sing, K.S.W.; Everett, D.H.; Haul, R.A.W.; Moscou, L.; Pierotti, R.A.; Rouquerol, J.; Siemieniewska, T. Reporting Physisorption Data for Gas/Solid Systems with Special Reference to the Determination of Surface Area and Porosity. *Pure Appl. Chem.* **1985**, *57*, 603–619. [CrossRef]
34. Anbia, M.; MooaviFard, S.E. Improving humidity sensing properties of nanoporous TiO_2 –10 mol % SnO_2 thin film by co-doping with La^{3+} and K^+ . *Sens. Actuator B-Chem.* **2011**, *160*, 215–221. [CrossRef]

Sample Availability: Samples of the compounds cobalt molybdate ($\beta-CoMoO_4$) are available from the authors.



© 2018 by the authors. Licensee MDPI, Basel, Switzerland. This article is an open access article distributed under the terms and conditions of the Creative Commons Attribution (CC BY) license (<http://creativecommons.org/licenses/by/4.0/>).